Extraction of One Time Point Dynamic Group Features via Tucker Decomposition of Multi-subject FMRI Data: Application to Schizophrenia

Yue Han[1], Qiu-Hua Lin[1(✉)], Li-Dan Kuang[2], Ying-Guang Hao[1], Wei-Xing Li[1], Xiao-Feng Gong[1], and Vince D. Calhoun[3]

[1] School of Information and Communication Engineering, Dalian University of Technology, Dalian 116024, China
qhlin@dlut.edu.cn

[2] School of Computer and Communication Engineering, Changsha University of Science and Technology, Changsha 410114, China

[3] Tri-Institutional Center for Translational Research in Neuroimaging and Data Science (TReNDS), Georgia State University, Georgia Institute of Technology, Emory University, Atlanta, GA, USA

Abstract. Group temporal and spatial features of multi-subject fMRI data are essential for studying mental disorders, especially those exhibiting dynamic properties of brain function. Taking advantages of a low-rank Tucker model in effectively extracting temporally and spatially shared features of multi-subject fMRI data, we propose to extract dynamic group features via Tucker decomposition for identifying patients with schizophrenia (SZs) from healthy controls (HCs). We segment multi-subject fMRI data using sliding-window technique with different lengths and step size of one time point, and analyze amplitude of low frequency fluctuations and voxel features for shared time courses and shared spatial maps obtained by Tucker decomposition of segmented data. Results of two-sample *t*-tests show that HCs have higher amplitudes of low frequency fluctuations within 0.01–0.08 Hz than SZs within window length of 40 s–160 s, and significant HC-SZ activation differences exist in such as the inferior parietal lobule and left part of auditory within 40 s window, providing new evidence for analyzing schizophrenia.

Keywords: Multi-subject fMRI data · One time point dynamic estimates · Group features · Low-rank Tucker decomposition · Schizophrenia

1 Introduction

Temporal and spatial group feature extraction is important in analyses of multi-subject functional magnetic resonance imaging (fMRI) data, which can provide evidence for studying mental disorders such as schizophrenia [1–6]. Blind source separation such as independent component analysis (ICA) has been widely used to extract group features

B. Luo et al. (Eds.): ICONIP 2023, CCIS 1963, pp. 518–527, 2024.
https://doi.org/10.1007/978-981-99-8138-0_41

including time courses (TCs) and spatial maps (SMs) from multi-subject fMRI data. TCs of interest can be used to form functional network connectivity (FNC) based on correlations [1, 2] or to calculate amplitude of low frequency fluctuations [3] for finding group differences. SMs of interest, e.g., the default mode network (DMN), can be directly used to identify spatial variations of SZs using statistical methods (F-test [4] or *t*-test [5]).

Extracting dynamic group features from multi-subject fMRI data can be promising, since human brain is a highly dynamic system [6]. Kiviniemi et al. [7] conducted ICA of fMRI data using sliding window of 60 time points and sliding step of one time point, and calculated correlations between group averaged DMN and its template for each window to find dynamic spatial variances of healthy participants. Dynamic group features can also be used to identify brain abnormalities. Lu et al. [2] obtained individual TCs by group ICA (GICA), used a sliding window with 15 time points and step size of one time point to have segmented TCs. Each window of segmented TCs from nine resting-state networks (e.g., DMN and visual network) were used to construct dynamic FNC to explore the aberrant of neurocognitive performance in patients with acute mild traumatic brain injury. Ma et al. [8] performed independent vector analysis (IVA) on segmented multi-subject fMRI data with 50 time points and 50% overlap and built dynamic FNC of SMs based on mutual information to find differences between health individuals and schizophrenia patients.

Group components with or without individual variability were extracted and utilized via the above-mentioned methods. In practice, group shared temporal and spatial information, simultaneously extracted with individual temporal and spatial information, is essential to fully analyze brain function of multi-subject fMRI data. Among blind source separation methods, Tucker decomposition (TKD), as one of the tensor decomposition algorithms, is characterized by fully utilization of tensor structure information of multi-subject fMRI data and the non-diagonal core tensor that carry out subject-specific information [9–11], so we hypothesize that the difference of static group features extracted by TKD can be largely improved by dynamic analyses. We proposed a sparse and low-rank Tucker model (slcTKD) for decomposing three-way (voxel $\times$ time $\times$ subject) multi-subject fMRI data [11]. The slcTKD model makes full use of tensor structure of multi-subject fMRI data to obtain group shared TCs and SMs, and individual information in the core tensor without compressing the original fMRI data.

Considering that extracting dynamic group shared features via slcTKD could provide new evidence for studying mental disease such as schizophrenia, we propose to extract one time point dynamic group features via slcTKD for identifying differences between patients with schizophrenia (SZs) and healthy controls (HCs). We select DMN and auditory cortex (AUD) as two components of interest since they have been verified to be biomarkers of schizophrenia [4, 5, 8]. First, we segment multi-subject fMRI data of HCs and SZs using sliding window with different lengths (20–140 time points) in steps of one time point. Then, we obtain shared TCs and shared SMs via slcTKD from segmented fMRI data. Next, we extract frequency features within multiple bands from shared TCs for all time windows based on amplitude of low-frequency fluctuations (i.e., averaged square root of the power spectrum within typical band: 0.01–0.08 Hz, slow-5 band: 0.01–0.027 Hz, and slow-4 band: 0.027–0.073 Hz for each shared TCs), and calculate

dynamic voxel features by performing dynamic voxel-level analysis on shared SMs. Finally, two-sample *t*-tests are conducted on the frequency features and voxel features between HCs and SZs to find significant differences with different window lengths. Since dynamic analysis on (voxel × time × subject) fMRI data via TKD has not been explored to our best knowledge, our findings within different window lengths can be promising in finding new evidences for identifying SZs.

To summarize, contributions of this study are three-fold:

(1) We propose to extract one time point dynamic group shared features via slcTKD for three-way (voxel × time × subject) fMRI data, and extract frequency and voxel features for finding significant temporal and spatial differences between HCs and SZs.
(2) We examine HC-SZ differences within a wide range of window lengths (20–140 time points) by using the strategy of one time point dynamic estimates.
(3) New temporal and spatial evidence for identifying SZs from HCs are found, e.g., HCs have higher amplitudes of low frequency fluctuations within 0.01–0.08 Hz for window lengths of 40 s–160 s; exhibit higher activations in left part of auditory (AL) but lower activations in right inferior parietal lobule (RIPL) within a window length of 40 s, compared with SZs.

2 Methods

2.1 The slcTKD Model

For a multi-subject fMRI data $\underline{\mathbf{X}} \in \mathbb{R}^{V\times T\times K}$, where V, T, K denote the number of in-brain voxels, time points, and subjects, the Tucker-2 model is built as follows:

$$\underline{\mathbf{X}} = \underline{\mathbf{G}} \times_1 \mathbf{S} \times_2 \mathbf{B} + \underline{\mathbf{E}} \tag{1}$$

where $\times_n$ denotes the mode-n product; $\mathbf{S} = [\mathbf{s}_1, \mathbf{s}_2, \ldots \mathbf{s}_N] \in \mathbb{R}^{V\times N}$ and $\mathbf{B} = [\mathbf{b}_1, \mathbf{b}_2, \ldots \mathbf{b}_N] \in \mathbb{R}^{T\times N}$ represent shared SM matrix and shared TC matrix; N is the model order; $\underline{\mathbf{G}} \in \mathbb{R}^{N\times N\times K}$ and $\underline{\mathbf{E}} \in \mathbb{R}^{V\times T\times K}$ are the core tensor and residual tensor. In slcTKD algorithm [11], the tensors and matrices are updated based on the following:

$$\min_{\mathbf{S},\mathbf{B},\underline{\mathbf{G}},\underline{\mathbf{E}}} \left\|\underline{\mathbf{X}} - \underline{\mathbf{G}} \times_1 \mathbf{S} \times_2 \mathbf{B} - \underline{\mathbf{E}}\right\|_{\mathbf{F}}^2 + \|\mathbf{S}\|_{\mathbf{F}}^2 + \|\mathbf{B}\|_{\mathbf{F}}^2 + \delta\|\mathbf{S}\|_p + \lambda\left\|\underline{\mathbf{G}}\right\|_1 + \gamma\left\|\underline{\mathbf{E}}\right\|_1 \tag{2}$$

where $\|\cdot\|_F$ denotes low-rank ℓ_F constraint, $\|\cdot\|_1$ and $\|\cdot\|_p$ are ℓ_1 and ℓ_p sparsity constraints ($0 < p \leq 1$), positive parameters δ, λ, and γ control the sparsity constraints effects. The model is solved by alternating direction method of multipliers and half quadratic splitting. More details of the updating of $\mathbf{B}$ and $\mathbf{S}$ can be referred to [11].

2.2 Extraction of Dynamic Group Shared Temporal and Spatial Components via Sliding Window and slcTKD

We denote a component of interest by a subscript of "*" (e.g., $\mathbf{b}_*$), and a component from the m th window by a superscript "m" (e.g., $\mathbf{b}^m$), where $m = 1, 2, ..., M$, and M is the total number of windows.

Given multi-subject fMRI data of HCs and SZs $\underline{\mathbf{X}}$, we divide T time points into M time windows $\left[\underline{\mathbf{X}}^1, \underline{\mathbf{X}}^2, \ldots, \underline{\mathbf{X}}^M\right]$, where $M = T - L + 1$, L is the window length, and $\underline{\mathbf{X}}^m \in \mathbb{R}^{V\times L\times K}$ is defined as $\underline{\mathbf{X}}^m = \underline{\mathbf{X}}(:, m : m + L - 1, :)$, $m = 1, 2, ..., M$. Then, for each $\underline{\mathbf{X}}^m$, we obtain $\mathbf{B}^m \in \mathbb{R}^{L\times N}$ and $\mathbf{S}^m \in \mathbb{R}^{V\times N}$ within each window using the slcTKD algorithm [11]. Next, we extract shared TCs and shared SMs of interest from $\mathbf{B}^m \in \mathbb{R}^{L\times N}$ and $\mathbf{S}^m \in \mathbb{R}^{V\times N}$ for analysis.

2.3 The Proposed Dynamic Group Features Extraction Method

Figure 1 shows extraction of dynamic temporal and spatial group features with DMN as an example. Group shared TCs of M windows are obtained by $\overline{\mathbf{B}} = \left[\mathbf{b}_*^1, \mathbf{b}_*^2, \ldots \mathbf{b}_*^M\right] \in \mathbb{R}^{L\times M}$, where $\mathbf{b}_*^m \in \mathbb{R}^L$ is the DMN component extracted from $\mathbf{B}^m$. Similarly, group shared SMs for DMN of M windows are defined by $\overline{\mathbf{S}} = \left[\mathbf{s}_*^1, \mathbf{s}_*^2, \ldots \mathbf{s}_*^M\right] \in \mathbb{R}^{V\times M}$, where $\mathbf{s}_*^m \in \mathbb{R}^V$ is the DMN component extracted from $\mathbf{S}^m$.

Dynamic Frequency Feature Extraction by Using Amplitudes of Low Frequency Fluctuations. For each $\mathbf{b}_*^m$, power spectrum is obtained by fast Fourier transform as follows:

$$\mathbf{p}^m(f) = \sum_l \mathbf{b}_*^m(l)\boldsymbol{e}^{\frac{-j2\pi lf}{L}} \tag{3}$$

where $\mathbf{p}^m \in \mathbb{C}^L$ is the power spectrum of $\mathbf{b}_*^m$, $l = 1, 2, ..., L$, $j = \sqrt{1}$, $f = 1, 2, ..., L$ denotes the frequency time point. Then the amplitude of low-frequency fluctuation of $\mathbf{b}_*^m$ within a specific frequency band is obtained as follows:

$$\tilde{\mathbf{b}}_*^m = \sum_{\tau(f)\in\Omega} \sqrt{\frac{|\mathbf{p}^m(f)|^2}{L}} \tag{4}$$

where $\tau(f)$ is the frequency in point f, $\tilde{\mathbf{b}}_*^m \in \mathbb{R}^1$ denotes the amplitude of low-frequency fluctuation, $\Omega = 0.01$–0.08 Hz (typical band) [12], 0.01–0.027 Hz (slow-5 band), or 0.027–0.073 Hz (slow-4 band) [13]. The dynamic temporal group features for all the M windows are collected by $\tilde{\mathbf{b}} = \left[\tilde{\mathbf{b}}_*^1, \tilde{\mathbf{b}}_*^2, \ldots, \tilde{\mathbf{b}}_*^M\right] \in \mathbb{R}^M$ for HCs and SZs, respectively, defined as $\tilde{\mathbf{b}}^{HC} \in \mathbb{R}^M$ and $\tilde{\mathbf{b}}^{SZ} \in \mathbb{R}^M$. Then two-sample t-tests are conducted to determine significant HC-SZ differences as follows:

$$\boldsymbol{t_b} = ttest\left(\tilde{\mathbf{b}}^{HC}, \tilde{\mathbf{b}}^{SZ}\right) \tag{5}$$

where $\boldsymbol{t_b} \in \mathbb{R}^1$ is the t-value, $ttest(\cdot)$ denotes two-sample t-test operation between HCs and SZs.

Dynamic Voxel Feature Extraction. The dynamic spatial group features are obtained by the vectorizing the same voxel values for M time windows, defined as $\bar{\mathbf{s}}_{(v)} = [\mathbf{s}_*^1(v), \mathbf{s}_*^2(v), \ldots, \mathbf{s}_*^M(v)] \in \mathbb{R}^M$, where $v = 1, 2, ..., V$. The voxel features extracted from HCs and SZs are defined as $\bar{\mathbf{s}}_{(v)}^{HC} \in \mathbb{R}^M$ and $\bar{\mathbf{s}}_{(v)}^{SZ} \in \mathbb{R}^M$, respectively, then two-sample t-tests are conducted between each voxel vectors to generate the HC-SZ difference t-map $\boldsymbol{t}_s \in \mathbb{R}^V$:

$$\boldsymbol{t}_{s(v)} = \Phi(v) \cdot ttest\left(\bar{\mathbf{s}}_{(v)}^{HC}, \bar{\mathbf{s}}_{(v)}^{SZ}\right) \tag{6}$$

where $\mathbf{\Phi} \in \mathbb{R}^V$ is a binary mask determined by the significant level, defined as:

$$\Phi(v) = \begin{cases} 1, \ if \left| ttest\left(\bar{\mathbf{s}}_{(v)}^{HC}, \bar{\mathbf{s}}_{(v)}^{SZ}\right)\right| > \boldsymbol{t}_{th} \\ 0, \ otherwise \end{cases} \tag{7}$$

where $\boldsymbol{t}_{th}$ is the threshold of t-value for two-sample t-test.

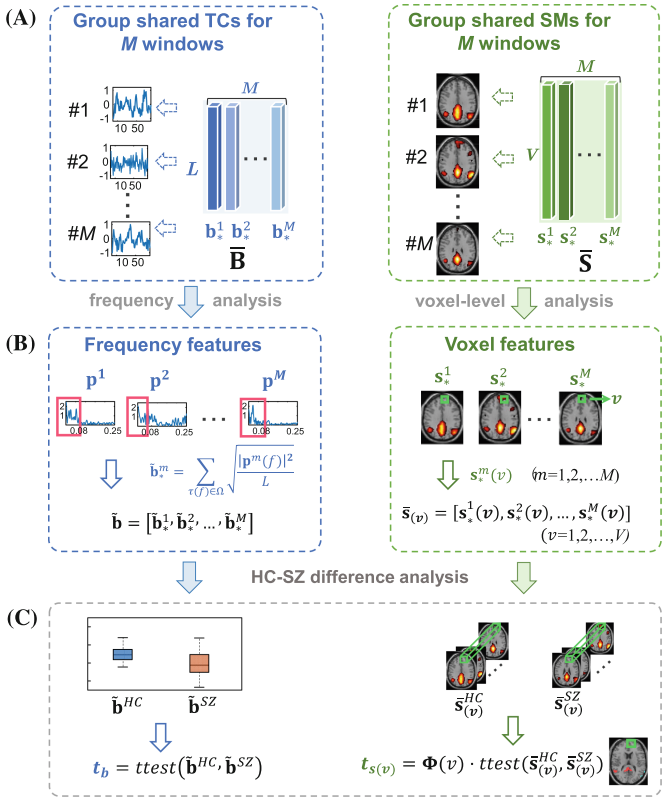

Fig. 1. Dynamic temporal and spatial group feature extraction of the proposed method. (A) Group shared TCs and SMs of M windows. (B) Dynamic frequency and voxel feature extraction. (C) Two-sample t-tests on dynamic features between HCs and SZs.

3 Experimental Methods

3.1 Resting-State fMRI Data

The resting-state fMRI data were collected from 10 HCs and 10 SZs with written subject consent overseen by the University of New Mexico Institutional Review Board. During the scan, all participants were instructed to rest quietly in the scanner, keeping their

eyes open without sleeping and not to think of anything in particular. FMRI scans were acquired using a 3.0 T Siemens Allegra scanner, equipped with 40 mT/m gradients and a standard quadrature head coil. The functional scan was acquired using gradient-echo echo-planar imaging with the following parameters: TR = 2 s, TE = 29 ms, field of view = 24 cm, acquisition matrix = 64 × 64, flip angle = 75°, slice thickness = 3.5 mm, slice gap = 1 mm. Data preprocessing was performed using the SPM software package (http://www.fil.ion.ucl.ac.uk/spm). Five scans were excluded due to steady state magnetization effects and 146 resting state scans were used for analysis. After motion correction, the functional images were normalized into Montreal Neurological Institute standard space. Following spatial normalization, the data were slightly sub-sampled to $3 \times 3 \times 3$ mm^3, resulting in $53 \times 63 \times 46$ voxels. Data were then spatially smoothed with an $8 \times 8 \times 8$ mm^3 full-width half-maximum (FWHM) Gaussian kernel. After removing the voxels out of the brain and flattening the volume image data of all time points for each subject, we construct the three-way fMRI data of size $62336 \times 146 \times 10$ for HCs and $62336 \times 146 \times 10$ for SZs, respectively.

3.2 Experimental Methods

In order to explore HC-SZ differences with a wide range of window lengths, we change L from 20 to 140 at an interval of 10. The model order is selected by $N = min(L, 40)$, since the components of interest cannot be well extracted with smaller model orders. Other parameters of slcTKD given in Eq. (2) are selected to be the same with those used in [11]. The references for DMN and AUD provided by Smith et al. [14] are used to select components of interest. Before extracting frequency features, each group shared TCs components are detrended and normalized to the range of 0 to 1. The t-values obtained from two-sample t-tests ($df = 2M - 2$, $p < 0.05$, corrected by false discovery rate) are utilized to evaluate the performance, and thresholds are changed for different L, ranging from $|t| = 1.969$ ($L = 20$, $M = 127$, $df = 252$) to $|t| = 2.179$ ($L = 140$, $M = 7$, $df = 12$).

4 Results

4.1 Dynamic Frequency Features of Group Shared TCs

Figure 2A shows multiple bands of results of t-values with different window lengths. We see that positive t-values are consistently obtained for the typical and slow-4 bands, indicating that HCs have higher amplitude of low-frequency fluctuation than SZs, agreeing with previous static analyses on raw fMRI data [15–17]. With the increase of L, the t-values show decreasing trend within the typical and slow-5 bands, while the changes are not obvious in slow-4 band. Significant differences ($p < 0.05$) are obtained within typical band when $L = 20$–80 (40 s–160 s) for both components, which extend the range of previous utilized window lengths in dynamic analyses (commonly 30 s–60 s) [6]. Figure 2B shows boxplots for amplitude of low-frequency fluctuations within the typical band 0.01–0.08 Hz for DMN and AUD when $L = 20$, 50, and 80. We see that the amplitude of low-frequency fluctuations within the typical band show less obvious HC-SZ differences with the increase of L.

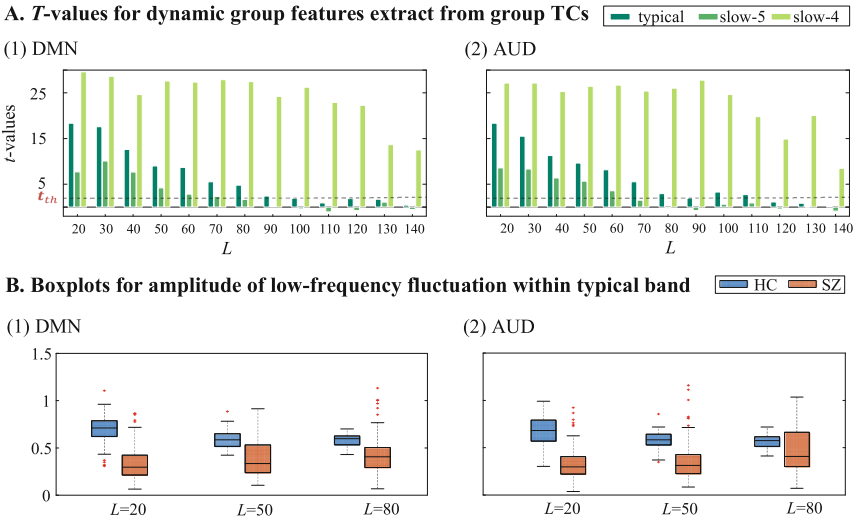

Fig. 2. Results of dynamic frequency features of group shared TCs. (A) Multiple bands of *t*-values of two sample *t*-test on dynamic temporal features between HCs and SZs. (B) Boxplots for amplitude of low-frequency fluctuation within the typical band. (1) DMN. (2) AUD. Thresholds of *t*-values t_{th} ($p < 0.05$) for each window length are marked by dotted lines (typical band: 0.01–0.08 Hz, slow-5 band: 0.01–0.027 Hz, slow-4 band: 0.027–0.073 Hz).

4.2 Dynamic Voxel Features of Group Shared SMs

Figure 3 shows voxel numbers inside the DMN and AUD reference masks with all window lengths and comparison of HC-SZ difference *t*-maps ($p < 0.05$) when $L = 20$, 50, and 80. Figure 3A1 also shows the voxel numbers inside anterior cingulate cortex (ACC) since it has been verified as a biomarker of SZs [4, 5]. HC-SZ differences exist in DMN when $L = 20$–130 (40 s–260 s), and in ACC when $L = 30$–100 (60 s–200 s). In addition, we also notice that SZs exhibit significantly larger activations in RIPL (see Fig. 3B), especially when $L = 20$ (40 s). Changes of IPL in SZs are also important [18], but previous findings are not exactly consistent, e.g., [19] found increased functional connectivity between RIPL with the right lingual gyrus and inferior occipital gyrus in SZs, while [20] showed decreased regional homogeneity in RIPL for SZs. This study provides new evidence for studying RIPL in SZs for dynamic analyses.

Significant HC-SZ differences are captured in AUD within $L = 20$–120 (40 s–240 s), especially when $L = 20$ in AL, as shown in Fig. 3C, indicating the abnormalities in AL of SZs [4] and verifying that AL is specialized for rapid temporal processing [21]. In addition, we newly find that significant differences exist in right part of auditory (AR) within larger window length (see Fig. 3C3–C4), which may be caused by the increasing activity of right temporal lobe to environmental sounds [22] and auditory hallucinations of SZs. These results indicate that different subcomponents have different sensitivities for different window lengths, i.e., different dynamic characteristics, suggesting the potential of one time point dynamic estimates for detailed investigation of HCs and SZs.

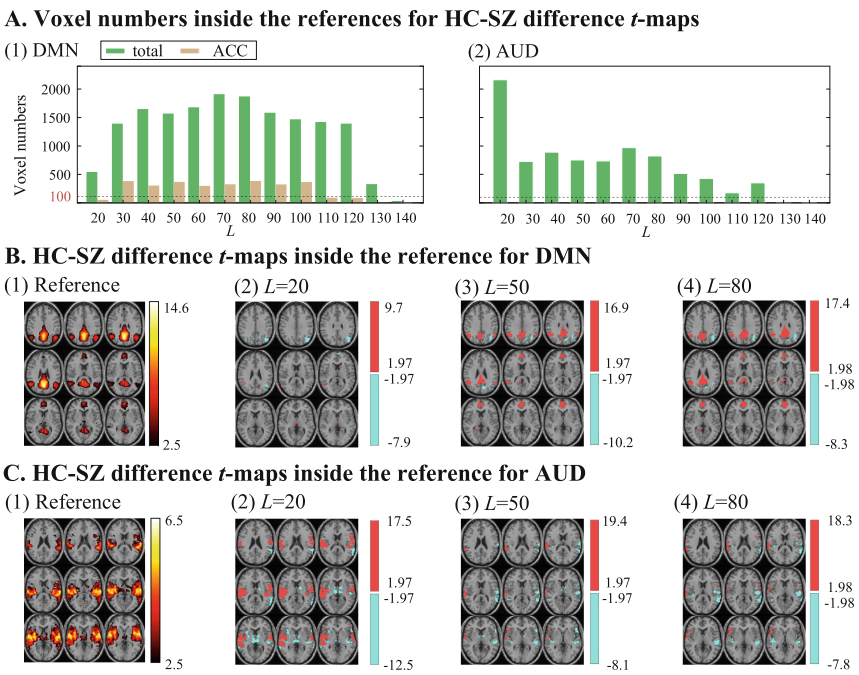

Fig. 3. Results of dynamic frequency features of group shared SMs. (A) Voxel numbers inside the references for HC-SZ difference *t*-maps. (1) DMN. (2) AUD. (B) HC-SZ difference *t*-maps inside the reference for DMN. (C) HC-SZ difference *t*-maps inside the reference for AUD. (1) Reference. (2) $L = 20$. (3) $L = 50$. (4) $L = 80$. Threshold of 100 voxels is marked by dotted lines.

5 Conclusion

In this study, one time point dynamic group shared frequency and voxel features are extracted via slcTKD for finding significant temporal and spatial differences between HCs and SZs, within a wide range of sliding window lengths (20–140 time points). Results show that HCs have significant higher amplitudes of low frequency fluctuations within 0.01–0.08 Hz than SZs for window lengths of 40 s–160 s, and significant HC-SZ activation differences are captured in subcomponents of DMN and AUD within specific lengths of window (e.g., ACC: 60 s–200 s, RIPL: 40 s, AL: 40 s). Compared to the existing group analysis algorithms such as GICA in [6] and IVA in [8], the proposed algorithm has two advantages: (1) TKD utilizes high dimensional structure of multi-subject fMRI data while GICA and IVA do not; (2) TKD can simultaneously extracts group shared spatial and temporal features while the existing algorithm cannot, thus, the group features extracted by TKD are more distinctive than those extracted by the existing algorithms. As a result, the dynamic frequency and voxel-level analyses proposed in this paper are better and more complete. Since slcTKD model can simultaneously provide subject-specific temporal and spatial features [11], we will also further extract dynamic subject-specific features for studying SZs together with shared features. Current results appear to show strong HC-SZ differences, we will evaluate on more subjects later.

Acknowledgement. This work was supported in part by the National Natural Science Foundation of China under Grants 61871067 and 62071082, the NSF under Grant 2112455, the NIH Grant R01MH123610, the Fundamental Research Funds for the Central Universities, China, under Grants DUT20ZD220 and DUT20LAB120, and the Supercomputing Center of Dalian University of Technology.

References

1. Sakoglu, U., Pearlson, G.D., Kiehl, K.A., Wang, Y.M., Michael, A.M., Calhoun, V.D.: A method for evaluating dynamic functional network connectivity and task-modulation: application to schizophrenia. Magn. Reson. Mater. Phys. Biol. Med. **23**(5–6), 351–366 (2010)
2. Lu, L., et al.: Aberrant static and dynamic functional network connectivity in acute mild traumatic brain injury with cognitive impairment. Clin. Neuroradiol. **32**(1), 205–214 (2022)
3. Qi, S., et al.: Multiple frequency bands analysis of large scale intrinsic brain networks and its application in schizotypal personality disorder. Front. Comput. Neurosci. **12**(64), 1–16 (2018)
4. Qiu, Y.: Spatial source phase: a new feature for identifying spatial differences based on complex-valued resting-state fMRI data. Human Brain Mapp. **40**(9), 2662–2676 (2019)
5. Kuang, L.D., Lin, Q.H., Gong, X.F., Cong, F., Sui, J., Calhoun, V.D.: Model order effects on ICA of resting-state complex-valued fMRI data: application to schizophrenia. J. Neurosci. Methods **304**, 24–38 (2018)
6. Fu, Z., et al.: Characterizing dynamic amplitude of low-frequency fluctuation and its relationship with dynamic functional connectivity: an application to schizophrenia. Neuroimage **180**, 619–631 (2018)
7. Kiviniemi, V., et al.: A sliding time-window ICA reveals spatial variability of the default mode network in time. Brain Connectivity **1**(4), 339–347 (2011)
8. Ma, S., Calhoun, V.D., Phlypo, R., Adalı, T.: Dynamic changes of spatial functional network connectivity in healthy individuals and schizophrenia patients using independent vector analysis. Neuroimage **90**, 196–206 (2014)
9. Kolda, T.G., Bader, B.W.: Tensor decompositions and applications. SIAM Rev. **51**(3), 455–500 (2009)
10. Han, Y., Lin, Q.H., Kuang, L.D., Gong, X.F., Cong, F., Calhoun, V.D.: Tucker decomposition for extracting shared and individual spatial maps from multi-subject resting-state fMRI data. In: IEEE International Conference on Acoustics, Speech and Signal Processing (ICASSP), pp. 1110–1114, June 2021
11. Han, Y., et al.: Low-rank Tucker-2 model for multi-subject fMRI data decomposition with spatial sparsity constraint. IEEE Trans. Med. Imaging **41**(3), 667–679 (2022)
12. Zang, Y.F., et al.: Altered baseline brain activity in children with ADHD revealed by resting-state functional MRI. Brain Develop. **29**(2), 83–91 (2007)
13. Zuo, X.N., et al.: The oscillating brain: complex and reliable. Neuroimage **49**(2), 1432–1445 (2010)
14. Smith, S.M., et al.: Correspondence of the brain's functional architecture during activation and rest. Nat. Acad. Sci. United States Am. **106**(31), 13040–13045 (2009)
15. Fryer, S.L., Roach, B.J., Wiley, K., Loewy, R.L., Ford, J.M., Mathalon, D.H.: Reduced amplitude of low-frequency brain oscillations in the psychosis risk syndrome and early illness schizophrenia. Neuropsychopharmacology **41**(9), 2388–2398 (2016)
16. Wang, X., et al.: Frequency-specific alteration of functional connectivity density in antipsychotic-naive adolescents with early-onset schizophrenia. J. Psychiatr. Res. **95**, 68–75 (2017)

17. Chang, M., et al.: Spontaneous low-frequency fluctuations in the neural system for emotional perception in major psychiatric disorders: amplitude similarities and differences across frequency bands. J. Psychiatry Neurosci. **44**(2), 132–141 (2019)
18. Torrey, E.F.: Schizophrenia and the inferior parietal lobule. Schizophr. Res. **97**(1–3), 215–225 (2007)
19. Liu, X., et al.: Selective functional connectivity abnormality of the transition zone of the inferior parietal lobule in schizophrenia, NeuroImage Clin. **11**, 789–795 (2016)
20. Wang, S., et al.: Abnormal regional homogeneity as a potential imaging biomarker for adolescent-onset schizophrenia: a resting-state fMRI study and support vector machine analysis. Schizophr. Res. **192**, 179–184 (2018)
21. Zatorre, R.J., Belin, P.: Spectral and temporal processing in human auditory cortex. Cereb. Cortex **11**(10), 946–953 (2001)
22. Hugdahl, K., Bronnick, K., Kyllingsbaek, S., Law, I., Gade, A., Paulson, O.B.: Brain activation during dichotic presentations of consonant-vowel and musical instrument stimuli: a 15O-PET study. Neuropsychologia **37**(4), 431–440 (1999)